

1 Onshore sandbar migration in the surf zone: new
2 insights into the wave induced sediment transport
3 mechanisms

A. Fernández-Mora¹, D. Calvete¹, A. Falqués¹, H.E. de Swart²

¹Department of Applied Physics,
Universitat Politècnica de
Catalunya-Barcelona Tech, Barcelona, Spain

²Institute for Marine & Atmospheric
research, Utrecht University, Utrecht, the
Netherlands

4 We present a novel process-based morphodynamic model, which includes
5 transport processes due to both velocity and acceleration skewness and a new
6 formulation for intra-wave motions, that successfully simulates observed of
7 onshore sandbar migration. Results confirm findings of previous studies, in
8 which each process was considered separately and in which sediment trans-
9 port was computed from the observed water motion. However, our results
10 indicate that accounting for the joint action of both velocity and accelera-
11 tion skewnesses causes major improvement of the modeled onshore bar mi-
12 gration, and is essential to accurately model the evolution of the entire cross-
13 shore bottom profile, when compared with observations. We also demonstrate
14 that the morphodynamics in the shoaling zone are dominated by velocity skew-
15 ness (bed-shear stresses), while sediment transport induced by acceleration
16 skewness (pressure gradients) controls the morphodynamics in the inner surf
17 zone.

1. Introduction

18 Surf zone sandbars are of primary importance for the persistence of sandy shores, as
19 they protect the beach during storms causing wave dissipation through wave breaking.
20 They also constitute a reservoir for the exchange of sand between the submerged and the
21 dry beach. Since the morphology of sandbars and the surf zone hydrodynamics are in-
22 trinsically coupled, understanding sandbar dynamics is important for coastal protection,
23 human activities (eg. industry, tourism, surfing, etc) or environmental issues (water qual-
24 ity, pollutant dispersion, biologic activity, etc). Sandbar morphodynamics has a strong
25 three-dimensional nature which is linked to wave-breaking, inducing horizontal circulation
26 in the surf zone (longshore current, rip currents). Despite the 3D nature of nearshore mor-
27 phodynamics, in many cases sandbars are remarkably longshore uniform and it is assumed
28 that cross-shore, rather than longshore processes, control the formation and migration of
29 bars.

30 There is general consensus with regard to the underlying mechanisms causing the off-
31 shore migration of sandbars: during storms, strong waves drive near-bottom intense off-
32 shore directed flow (undertow) that moves bars offshore [*Short*, 1999]. In contrast, the
33 mechanics of onshore sandbar migration is still a controversial topic. Under low energetic
34 conditions, currents are weak, and sediment transport is driven mostly by near-bottom
35 wave orbital motion. However, early attempts to simulate onshore sandbar migration
36 using wave-averaged sediment transport parameterizations based on bottom stresses (e.g.
37 Meyer-Peter and Müller power law) were not successful [*Roelvink and Stive*, 1989; *Wright*
38 *et al.*, 1991; *Thornton and Humiston*, 1996; *Rakha et al.*, 1997; *Gallagher et al.*, 1998]. It

39 was argued by *Elgar et al.* [2001] that this discrepancy was due to the sediment transport
40 formulation, which considers velocity skewness but no acceleration skewness (skewness
41 is here defined as the wave-averaging of the third power of a variable). This was con-
42 firmed by *Hoefel and Elgar* [2003] who used a bedload sediment transport proxy based
43 on the acceleration skewness developed by *Drake and Calantoni* [2001] to successfully
44 model an observed onshore sandbar migration event during the Duck94 experiment at
45 the Field Research Facility - USACE Army at Duck, North Carolina, USA. The contri-
46 bution of *Hoefel and Elgar* [2003] suggested that acceleration skewness was indispensable
47 to correctly model onshore bar migration.

48 Interestingly, *Hsu et al.* [2006] were also able to model onshore migration for the same
49 event using a modified energetic-based sediment transport that distinguishes the action
50 of the wave stirring in sediment transport from the action of waves plus currents. As
51 a result, it is unclear which mechanism, velocity or acceleration skewness, is the main
52 driver of onshore sandbar migration. *Hoefel and Elgar* [2003] and *Hsu et al.* [2006] ob-
53 tained their results by calculating the sediment transport from measured near bottom
54 velocities (3 hours averaged) of current meters at 40-100 cm from the bottom during the
55 Duck94 experiment. These models use the hydrodynamic measurements taken on the real
56 bathymetry to compute bottom changes. As real and computed bathymetry may diverge,
57 these models do not address the morphodynamic coupling and thus lack on the forecasting
58 abilities of fully process-based morphodynamical models.

59 Such process-based models are nowadays available and they include a detailed descrip-
60 tion of the intra-wave motion. In the framework of wave-averaged and depth-integrated

61 models, a parametrization that accurately describes that motion is a key factor. *Ruessink*
62 *et al.* [2012] used an adjusted version of the parameterization for orbital motion of *Abreu*
63 *et al.* [2010] to compute the morphological change of a cross-shore profile by using the
64 CROSMOR model [*Van Rijn*, 2007a, b] for a 5 days simulation under steady wave forcing.
65 They succeeded to model onshore sandbar migration patterns and, in this sense, their re-
66 sults encourage the use of this approximation as a plausible way to include wave skewness
67 and asymmetry effects on sediment transport computation in beach evolution models.
68 *Van der Werf et al.* [2012], using the *Ruessink et al.* [2012] parameterization, tested a to-
69 tal load transport formula against experimental data [*Roelvink and Reniers*, 1995; *Grasso*
70 *et al.*, 2011]. In this line, *Fernandez-Mora et al.* [2013] considered the extended energetic
71 model of *Hsu et al.* [2006] and the intra-wave parameterization of *Ruessink et al.* [2012] to
72 model bar migrations during 72 days at Duck, North Carolina, USA. Similarly, *Dubarbier*
73 *et al.* [2013], also by using the approach for the intra-wave motion, combined the transport
74 of *Hoefel and Elgar* [2003] and *Hsu et al.* [2006], to model the observed migration of a bar
75 in a flume.

76 However, those papers did not examine the joint action of both wave velocity and wave
77 acceleration skewness comparing the role of each one on onshore sandbar migration mech-
78 anism. Consequently, in this study a morphodynamic process-based model is used that
79 accounts for the intra-wave orbital velocity approximation of *Ruessink et al.* [2012] and in-
80 cludes the two main drivers of sediment transport, i.e., velocity skewness and acceleration
81 skewness. A third sediment transport formulation that combines those sediment trans-
82 port formulas is presented as well. Following the research of *Hoefel and Elgar* [2003] and

83 *Hsu et al.* [2006], the process-based model is used to model the onshore migration event
84 of Duck94. The three sediment transports are calibrated separately to obtain the best fit
85 for this event. A comparison of the results of the three transports is done for two main
86 purposes. Firstly, to confirm the results of *Hoefel and Elgar* [2003] and *Hsu et al.* [2006]
87 with a process-based model. That is, sediment transport formulations based on either
88 velocity skewness or on acceleration skewness can reproduce the onshore sandbar migra-
89 tion and, therefore, both processes may act in nature with similar effects. The second
90 purpose is to elucidate which is the role of velocity skewness and acceleration skewness in
91 the mechanism of onshore sandbar migration. The model will be introduced in the next
92 section. Afterwards, numerical results and discussion will be presented, followed by the
93 conclusions.

2. Numerical model and set-up

2.1. Model

94 The process-based model considers depth- and wave-averaged momentum and mass
95 balance equations coupled with wave- and roller-energy conservation, Snell's law and the
96 dispersion relationship [see *Fernandez-Mora et al.*, 2013, for detailed information]. The
97 formulation of *Ruessink et al.* [2012], adapted from *Abreu et al.* [2010], is used to model
98 the intra-wave near-bottom velocity, that is function of the root mean squared wave-height
99 H , the wave period T and the depth D . Time and depth-averaged undertow is computed
100 from mass transport due to wave and surface rollers. A detailed description of the model
101 formulation is given in the Auxiliary Material.

102 The bottom evolution is governed by the sediment mass conservation equation, which
 103 in the present context (longshore uniformity) reads

$$104 \quad (1 - n) \frac{\partial z_b}{\partial t} + \frac{\partial Q_x}{\partial x} = 0 \quad (1)$$

105 Here, z_b is the bed level, t is time, n is the porosity of sediment (set to 0.4) and Q_x is the
 106 wave-averaged sediment transport in the cross-shore direction. The x -axis points in the
 107 seaward direction.

108 To determine which is the governing mechanism driving onshore sandbar migration
 109 process, sediment transport is computed considering two transport formulas, one related
 110 to velocity skewness [*Hsu et al.*, 2006] and the other one related to acceleration skewness
 111 [*Hoefel and Elgar*, 2003].

112 2.1.1. The velocity skewness transport (SkV)

113 The velocity skewness transport (hereinafter SkV transport) follows the sediment trans-
 114 port description given by *Hsu et al.* [2006] complemented with a diffusive transport term
 115 Q_D . It is defined as

$$116 \quad Q_{SkV} = Q_V + Q_C + Q_D \quad (2)$$

117 in which Q_V and Q_C are the net sediment transport due to waves and currents given by
 118 *Hsu et al.* [2006], respectively:

$$119 \quad Q_V = \frac{C_w}{(s - 1)g} \left(\frac{\varepsilon_B}{\tan \varphi} \langle |\vec{U}_0|^2 U_{0,x} \rangle + \frac{\varepsilon_S}{W_0} \langle |\vec{U}_0|^3 U_{0,x} \rangle \right) \quad (3)$$

$$120 \quad Q_C = \frac{C_c}{(s - 1)g} \left(\frac{\varepsilon_B}{\tan \varphi} \langle |\vec{U}_t|^2 \rangle U_x + \frac{\varepsilon_S}{W_0} \langle |\vec{U}_t|^3 \rangle U_x \right) \quad (4)$$

122 Here, s is the specific gravity (set to 2.65), g is the acceleration due to gravity, φ is the
 123 friction angle ($\tan \varphi = 0.63$); ε_B and ε_S are transport efficiency factors (set to $\varepsilon_B = 0.135$)

124 and $\varepsilon_S = 0.015$ [Thornton and Humiston, 1996; Gallagher et al., 1998]), W_0 is the sediment
 125 fall velocity, \vec{U}_0 is the wave orbital velocity vector, \vec{U}_t is the total velocity vector (waves
 126 plus currents) and \vec{U} is the current velocity vector, related to the longshore current and
 127 the offshore directed undertow velocity. Subscript x indicates the cross-shore component.
 128 Vertical bars indicate the magnitude of the vector and the angular brackets $\langle \rangle$ the time-
 129 averaging of the vector. Note that these sediment transport terms neglect settling lag
 130 effects, and thus, the transport related to the Stokes drift is not considered, as was done
 131 in Henderson et al. [2004]. Values of the waves and currents friction coefficients C_w and C_c
 132 will be calibrated by fitting the SkV transport model results with observations, to verify
 133 that a sediment transport formula based on velocity skewness can explain the onshore
 134 migration of the bar.

135 The term Q_D in equation 2 represents a diffusive transport resulting from the tendency
 136 of sand to move downslope:

$$137 \quad Q_D = \lambda_d \nu(x) \left(\frac{1}{\tan \varphi - dz_b/dx} \right) \left(\frac{dz_b/dx}{\tan \varphi} \right) \quad (5)$$

138 where dz_b/dx is the bottom slope, λ_d is a coefficient to be set in the calibration, together
 139 with the friction coefficients C_w and C_c , and ν is a term that is specified in the Auxiliary
 140 Material.

141 **2.1.2. The acceleration skewness transport (SkA)**

142 The acceleration skewness transport model (hereinafter SkA transport) is based on the
 143 model of Hoefel and Elgar [2003], complemented with the transport due to mean currents
 144 (Q_C) and the diffusive transport (Q_D) as are given in equations 4 and 5, respectively, to
 145 provide a more accurate description of the physics involving sediment transport processes.

146 The SkA transport reads

$$147 \quad Q_{SkA} = Q_A + Q_C + Q_D \quad (6)$$

148 Here Q_A is the acceleration-driven transport given by *Hoefel and Elgar* [2003]:

$$149 \quad Q_A = \begin{cases} K_a(a_{spike,x} - \text{sign}(a_{spike,x})a_{cr}) & a_{spike,x} \geq a_{cr} \\ 0 & a_{spike,x} < a_{cr} \end{cases} \quad (7)$$

150 in which K_a is a constant ($m\ s$), a_{cr} is the threshold acceleration (set to $0.5\ \text{ms}^{-2}$) and
 151 $a_{spike} = \langle a(t)^3 \rangle / \langle a(t)^2 \rangle$, which is related to the acceleration skewness [*Drake and Calan-*
 152 *toni*, 2001]. Although the original expression of the *Hoefel and Elgar* [2003] formula
 153 accounted just for the bed-load contribution, in the present work it is assumed that the
 154 K_a constant accounts for the contribution of both bedload and suspended load. Sub-
 155 script x indicates the cross-shore component. The acceleration $\vec{a}(t)$ is computed as the
 156 local time derivative of the total velocity \vec{U}_t . Similarly as for the SkV transport, K_a ,
 157 C_c and λ_d are parameters to be calibrated by fitting results of the SkA transport model
 158 with observations, in order to address that acceleration skewness can explain the onshore
 159 migration.

160 **2.1.3. The combined transport (MiX)**

161 In order to account for all previous transport terms, a new sediment transport formula-
 162 tion is considered that combines the SkV and the SkA transport formulas and therefore
 163 contains the terms Q_V , Q_A , Q_C and Q_D of equations (3), (4), (5) and (7). To system-
 164 atically analyze the relative importance of the velocity skewness and the acceleration
 165 skewness on onshore sandbar migration, the new sediment transport model (hereinafter
 166 MiX transport) is defined in terms of the SkV and the SkA transports as follows:

$$\begin{aligned}
167 \quad Q_{MiX} &= \alpha_V Q_V^{SkV} + \alpha_A Q_A^{SkA} + \beta[\alpha_V Q_C^{SkV} + \alpha_A Q_C^{SkA}] \\
168 \quad &+ \gamma[\alpha_V Q_D^{SkV} + \alpha_A Q_D^{SkA}]
\end{aligned} \tag{8}$$

169 In the expression above, the superscripts SkV and SkA denote, respectively, the sedi-
170 ment transport terms from the SkV and the SkA models once they have been calibrated
171 separately. The coefficients α_V , α_A , β and γ are four independent coefficients that weight
172 the different transport terms. The coefficients α_V and α_A weight the amount of the
173 action of velocity skewness and acceleration skewness on the MiX transport, in such a
174 way that the set $[\alpha_V, \alpha_a, \beta, \gamma] = [1, 0, 1, 1]$ is the calibrated SkV transport, and the set
175 $[\alpha_V, \alpha_a, \beta, \gamma] = [0, 1, 1, 1]$ leads to the calibrated SkA transport. The optimum values
176 of the four coefficients $[\alpha_V, \alpha_A, \beta, \gamma]$ will result from a calibration with observed onshore
177 sandbar migration.

2.2. Data, experimental setup and calibration

178 The test period concerns the onshore sandbar migration event during the Duck94 field
179 experiment at the Field Research Facility (FRF) at Duck, NC [*Gallagher et al.*, 1998;
180 *Elgar et al.*, 2001]. This sequence is characterized by a 30 m onshore migration of the
181 sandbar under relatively low energy wave conditions from 21st to 28th September 1994.
182 The hydrodynamics of the model are initialized with the cross-shore profile bathymetry of
183 21st September and are driven with the wave data sampled by the 8-m water depth, 925 m
184 offshore FRF pressure gauges that supply the RMS wave heights, period and direction
185 each 3 hours during the Duck94 experiment, and the water level is given by the NOAA
186 pressure gauge at the end of the FRF pier (sampled each 6 minutes).

187 The hydrodynamics and the morphological change are computed every 300 s over a
 188 non-uniform grid. Sand grain diameter is considered constant along the profile and set
 189 to $d_{50} = 0.2$ mm with the corresponding settling velocity $W_0 = 0.025$ ms⁻¹ [*Hsu et al.*,
 190 2006]. Hydrodynamics parameters are set according to previous calibrations [*Fernandez-*
 191 *Mora et al.*, 2013], using the wave height, set-up and longshore currents data along 10
 192 cross-shore profiles and 39 wave conditions during the SandyDuck'97 experiment at the
 193 FRF-Duck, NC.

194 The model skill is quantified through a 'Brier skill score' type parameter [*Van Rijn*
 195 *et al.*, 2003; *Ruessink*, 2005] defined as

$$196 \quad S = 1 - \frac{\int_{x_1}^{x_2} (z_b(x) - z_{b,obs}(x))^2 dx}{\int_{x_1}^{x_2} (z_{b,obs}(x) - z_{b0,obs}(x))^2 dx} \quad (9)$$

197 where $z_b(x)$ is the bottom elevation computed by the model at the end of the event (28th
 198 September, 1994), $z_{b,obs}(x)$ is the observed bottom elevation at that date, $z_{b0,obs}(x)$ is
 199 the observed elevation at the beginning of the event (21st September 1994) along the
 200 cross-shore direction x , and x_1 and x_2 limit the cross-shore profile zone where the skill
 201 is computed. The values of the skill S range within $[-\infty < S \leq 1]$. Perfect agreement
 202 between results and observations is given by a $S = 1.0$. Values $0 < S < 1$ correspond to
 203 better simulations than assuming no-bottom change ($S = 0$).

204 As the aim of the present work is focused on sandbar morphodynamics, the skill S is
 205 considered along the bar zone $S_{bar} = S(185 \text{ m}, 265 \text{ m})$. In addition, the S related to the
 206 inner zone $S_{in} = S(155 \text{ m}, 185 \text{ m})$, the offshore zone $S_{off} = S(265 \text{ m}, 335 \text{ m})$ and the
 207 entire profile $S_{tot} = S(155 \text{ m}, 335 \text{ m})$ will be considered as well.

208 The SkV and SkA transports are calibrated to maximize the skill S_{bar} for the Duck94
 209 onshore sandbar migration event. The sediment transport parameters are considered in
 210 the following ranges: the waves and currents friction coefficients C_w and C_c from 0 to
 211 5×10^{-3} , the K_a constant from 0 to 1×10^{-3} m s and the coefficient λ_d from 0 to 1×10^{-2} .
 212 The set of parameters achieving the global maximum value of S_{bar} are considered the best
 213 fitting parameters for the SkV and SkA transport models. Using these parameters, the
 214 MiX transport is calibrated ranging the weighting parameters α_V , α_A , β , and γ from 0 to
 215 1.50 to get the maximum value of S_{bar} .

3. Results and Discussion

216 With the best fits for the SkV transport ($C_w = 3.9 \times 10^{-4}$, $C_c = 1.0 \times 10^{-5}$, $\lambda_d = 3.0 \times$
 217 10^{-3}) and for the SkA transport ($K_a = 1.4 \times 10^{-5}$ m s, $C_c = 1.4 \times 10^{-4}$, $\lambda_d = 4.2 \times 10^{-4}$)
 218 , both bar crest position and growth are properly reproduced (see Figures 1a and 1b.). In
 219 terms of the skill of each model, the result for the SkV transport is slightly more accurate
 220 than the one obtained with the SkA transport ($S_{bar}^{SkV} = 0.965$ and $S_{bar}^{SkA} = 0.955$). This
 221 yields to our first and second key results: i) the process-based model confirms the findings
 222 of *Hoefel and Elgar* [2003] and *Hsu et al.* [2006] and, ii) supports the considerations of
 223 *Hsu et al.* [2006] that indeed both sediment transport mechanisms can yield the onshore
 224 bar migration.

225 Note that each transport mechanism leads to different behavior outside the sandbar
 226 zone. The SkA transport performs quite better in the inner region, reproducing the near-
 227 shore erosion, but overestimates the erosion on the bar seaward face. On the contrary, the
 228 SkV performs better in the outer region, although it is not able to simulate the near-shore

erosion and the trough shape. These behaviors have been quantified (see Table 1) by the skill in the inner surf zone (S_{in}), the shoaling zone (S_{out}) and for the entire profile (S_{tot}). Beach profile evolution for the Duck94 onshore event is also computed using the MiX transport.

Considering the best fits for the MiX transport, the model reproduces accurately the crest position and depth of the sandbar and trough shape (Figure 1c). The best fit is given by $\alpha_V = 0.45$ and $\alpha_A = 0.45$ and has a maximum skill of $S_{bar}^{MiX} = 0.981$, larger than the SkV and the SkA skill values. Furthermore, when the rest of the profile is considered (see S_{in} , S_{out} and S_{tot} in Table 1) the MiX transport achieves the overall best performance. The bed changes due to the MiX transport captures the best trends of the ones related to the SkA and the SkV transports, collecting both behaviors on modeling the inner surf-zone and shoaling zone shapes (see Figure 1.c). In this sense, their joint action is essential to model accurately the evolution of the entire profile during this onshore sandbar migration event.

This is further evidenced by analyzing the contribution of each term of the MiX transport in the bottom change (see Figure 2). At the Duck94 onshore sandbar migration event, the bottom evolution modeled with the MiX transport is characterized by a continuous onshore bar migration (Figure 2 E), as a result of an ongoing erosion on the offshore part of the bar and the deposition in the onshore part (Figure 2 F). The main drivers of the erosion-deposition pattern in the vicinity of the bar crest are the velocity and acceleration terms of the MiX transport, Q_V and Q_A (first and second terms on the RHS of Equation 8). The bottom changes of both components show a similar cross-shore pattern (Figure

251 2 G and H). The bed changes driven by the divergence of the sediment transport due to
252 currents Q_C (third term of Equation 8) are weaker (an order of magnitude lower than
253 the Q_V and Q_A terms), and correspond to erosion in the inner face of the sandbar and
254 accretion in the outer zone (Figure 2 I). The diffusive transport term Q_D (fourth term of
255 Equation 8) produces the flattening of the sandbar (Figure 2 J). During this event the
256 suspended-load transport components of the MiX transport are more relevant than the
257 bed-load transport terms (see Auxiliary Material). Summarizing, our third relevant find-
258 ing is that velocity skewness and acceleration skewness on the sediment transport should
259 be both accounted for.

260 Our fourth important finding is that the morphodynamics of the shoaling zone is mainly
261 driven by the velocity skewness (related to bed-shear stresses), while the morphodynamics
262 of the inner surf zone is mainly controlled by acceleration skewness [related to pressure
263 gradients, see *Foster et al.*, 2006]. This could be expected because in the shoaling zone,
264 wave-induced velocities become skewed, as wave surface changes from a sinusoidal to a
265 pitched-forward face shape; onshore velocities are stronger than offshore velocities, and
266 the sediment is then driven onshore. Indeed, field experiments [*Marino-Tapia et al.*,
267 2007] have shown that velocity skewness is the main transport mechanism in the shoaling
268 zone. On the other hand, as the waves approach the breaking point, usually near the
269 bar crest, wave velocity asymmetry increases producing strong accelerations that move
270 sediment onshore. The action of near-bed accelerations driving sediment onshore has been
271 analyzed by *Foster et al.* [2006]. They provided field evidence that the incipient sediment
272 motion is induced by fluid accelerations driven by pressure gradients. Therefore, both

273 velocity skewness and acceleration skewness can act together in nature and provide the
 274 physical background of the MiX transport.

To substantiate our fourth point, the wave-averaged magnitudes of the Shields parameter θ' and the Sleath parameter Sl are considered. They are given by

$$\theta' = \frac{1/2\rho f_{cw} \langle |\vec{U}_t| |U_{t,x}| \rangle}{(\rho_s - \rho)gd_{50}} \quad (10)$$

and

$$Sl = \frac{\rho \langle (\partial|U_{t,x}|/\partial t) \rangle}{(\rho_s - \rho)gd_{50}} \quad (11)$$

275 where, ρ is the water density, ρ_s is the sediment density and f_{cw} is the wave and currents
 276 friction factor (set to 0.02). The Shields parameter θ' (non-dimensional bed-shear stress) is
 277 related to the magnitude of the near-bottom velocity, and therefore, to the SkV transport.
 278 The Sleath parameter is related to the local derivative of the near-bottom velocity and
 279 thus, to the SkA transport. Values of the bottom changes, the θ' and Sl parameters and
 280 their corresponding gradients during the event are shown in Figure 3. During all the event,
 281 the bed-shear stresses action in the outer zone of the profile results in the bottom changes
 282 in this zone (Figure 3 A, B, D and F). Eventually, under the high energy conditions
 283 during 22nd September (Figure 2), pressure gradients increase in the outer zone. At low
 284 energy conditions (from 23rd to 26th September), the bottom change in the offshore zone
 285 is dominated by the action of bed-shear stresses. In the bar crest, both bed-shear stresses
 286 and pressure gradients are present, showing the back and forth action of the pressure
 287 gradients as tides rise or fall, respectively. This is consistent with the fact that during the
 288 low tide, the bar is in the inner surf zone while during the high tide it is in the shoaling
 289 zone. Finally the results of the last stage (moderate wave heights conditions) clearly show

290 that Sl is dominant respect to the action of θ' in the inner surf zone ($155 \text{ m} < x < 185 \text{ m}$).

291 On contrary, in the the outer zone ($x > 265 \text{ m}$) bed-shear stresses are dominant.

292 Since it has been demonstrated that the wave velocity and acceleration skewness play
293 a key role on modeling the onshore sandbar migration, the modeled intra-wave motion
294 has been compared with measurements in terms of these characteristics. The comparison
295 shows that there is a good agreement between both intra-wave motions (detailed in the
296 Auxiliary Material). Lastly, it should be noted that additional experiments, in which the
297 acceleration $\vec{a}(t)$ is computed as the total time derivative of \vec{U}_t instead of using the local
298 time derivative, lead to similar results.

4. Conclusions

299 With the help of a full process-based morphodynamic model, it has been shown that
300 accounting for the joint action of both velocity and acceleration skewnesses causes major
301 improvement of the modeled onshore bar migration, and is essential to accurately model
302 the evolution of the entire cross-shore bottom profile. The sediment transport has a
303 remarkable spatial dependence with regard to the wave propagation along the profile.
304 Two regions should be distinguished: the shoaling zone, where the velocity skewness
305 dominates the sediment transport that is mainly induced by bed-shear stresses, and the
306 breaking and inner surf zone, where the acceleration skewness dominates and sediment
307 transport is mainly induced by pressure gradients.

308 Moreover, model results confirm that sediment transport based either solely on velocity
309 skewness or acceleration skewness achieve to accurately reproduce the onshore sandbar
310 migration, yet they can lead to significant mismatches away from the bar zone. Therefore,

311 results in which sediment transport was computed from the observed velocities and for
312 which both the velocity [*Hsu et al.*, 2006] and acceleration [*Hoefel and Elgar*, 2003] skew-
313 ness can cause the onshore sandbar migration are confirmed. In order to achieve good
314 results, it is necessary to describe realistically [*Abreu et al.*, 2010; *Ruessink et al.*, 2012]
315 the intra-wave orbital motion in process-based models.

316 All these findings are subject to some limitations to be considered. One of the main
317 assumptions on beach profile evolution models is the alongshore uniformity. In this sense,
318 the alongshore variations in bathymetry induce variations in the wave properties and in
319 the currents, affecting the cross-shore transport and originating gradients in the longshore
320 transport, and this has been disregarded. Moreover, the results presented here are, like
321 the previous works of *Hoefel and Elgar* [2003] and *Hsu et al.* [2006], site-specific and are
322 focused on one short event with mostly normal wave incidence. On the other hand, on
323 testing the model under high energy conditions to reproduce an offshore migration event,
324 the model can simulate the seaward migration linked to the sandbar decay but not a pure
325 offshore migration. Further research should validate the present findings on the effects of
326 velocity and acceleration skewness on sediment transport for different geomorphic settings
327 and wave conditions.

328 **Acknowledgments.** Data are provided by the Field Research Facility, Field Data
329 Collections and Analysis Branch, US Army Corps of Engineers, Duck, North Carolina. We
330 acknowledge funding from the Spanish research projects CTM2009-11892 and CTM2012-
331 35398. The authors wish to thank to Dr. G. Coco for his valuable comments and

332 suggestions on the manuscript and to Dr. F. Ribas for providing us the challenge to
333 initiate this research.

References

- 334 Abreu, T., P. A. Silva, F. Sancho, and A. Temperville (2010), Analytical approximate
335 wave form for asymmetric waves, *Coastal Eng.*, *657*, 656–667.
- 336 Drake, T. G., and J. Calantoni (2001), Discrete particle model for sheet flow sediment
337 transport in the nearshore, *J. Geophys. Res.*, *106*(C9), 19,859–19,868.
- 338 Dubarbier, B., B. Castelle, V. Marieu, and G. Ruessink (2013), Numerical mod-
339 elling of pronounced sloping beach profile evolution: comparison with the large-scale
340 BARDEX II experiment, *J. Coastal Res.*, *SI 65*(1762-1767), iISSN 0749-0208.
- 341 Elgar, S., E. L. Gallagher, and R. T. Guza (2001), Nearshore sandbar migration, *J.*
342 *Geophys. Res.*, *106*(C6), 11,623–11,628.
- 343 Fernandez-Mora, A., D. Calvete, A. Falques, F. Ribas, and D. Idier (2013), On the pre-
344 dictability of mid-term cross-shore profile evolution, *J. Coastal Res.*, *SI 65*(476-481),
345 iISSN 0749-0208.
- 346 Foster, D. L., A. J. Bowen, R. A. Holman, and P. Nattoo (2006), Field evidence
347 of pressure gradient induced incipient motion, *J. Geophys. Res.*, *111*(C05004),
348 doi:10.1029/2004JC002863.
- 349 Gallagher, E., S. Elgar, and R. T. Guza (1998), Observations of sand bar evolution on a
350 natural beach, *J. Geophys. Res.*, *103*(C2), 3203–3215.
- 351 Grasso, F., H. Michallet, and E. Barthelemy (2011), Sediment transport associated with
352 morphological beach changes forced by irregular asymmetric, skewed waves, *J. Geophys.*

- 353 *Res.*, 116(C03020).
- 354 Henderson, S. M., J. S. Allen, and P. A. Newberger (2004), Nearshore sandbar migration
355 predicted by an eddy-diffusive boundary layer model, *J. Geophys. Res.*, 109(C06024),
356 doi:10.1029/2003JC002137.
- 357 Hoefel, F., and S. Elgar (2003), Wave-induced sediment transport and sandbar migration,
358 *Science*, 299, 1885–1887.
- 359 Hsu, T., S. Elgar, and R. T. Guza (2006), Wave-induced sediment transport and onshore
360 sandbar migration, *Coastal Eng.*, 53, 817–824.
- 361 Marino-Tapia, I., P. Russell, T. O’Hare, M. Davidson, and D. Huntley (2007), Cross-shore
362 sediment transport on natural beaches and its relation to sandbar migration patterns:
363 1. field observations and derivation of a transport parameterization, *J. Geophys. Res.*,
364 112(C03001), doi:10.1029/2005JC002893.
- 365 Rakha, K., R. Deigaard, and I. Broker (1997), A phase-resolving cross-shore sediment
366 transport model for beach profile evolution, *Coastal Eng.*, 31, 231–261.
- 367 Roelvink, J., and A. Reniers (1995), Report h2130. lip 11d delta flume experiments. a
368 data set for profile model validation, *Tech. rep.*, Delft Hydraulics, The Netherlands.
- 369 Roelvink, J. A., and M. J. F. Stive (1989), Bar-generating cross-shore flow mechanisms
370 on a beach, *J. Geophys. Res.*, 94(C4), 4785–4800.
- 371 Ruessink, B. G. (2005), Predictive uncertainty of a nearshore bed evolution model, *Con-*
372 *tinental Shelf Res.*, 25, 1053–1069.
- 373 Ruessink, B. G., G. Ramaekers, and L. C. van Rijn (2012), On the parameterization of
374 the free-stream non-linear wave orbital motion in nearshore morphodynamic models,

- 375 *Coastal Eng.*, 85, 56–63.
- 376 Short, A. D. (1999), *Handbook of Beach and Shoreface Morphodynamics*, Wiley, Chich-
377 ester.
- 378 Thornton, B., and R. T. Humiston (1996), Bar/trough generation on a natural beach, *J.*
379 *Geophys. Res.*, 101(C5), 12,097–12,110.
- 380 Van der Werf, J., H. Nomdem, J. Ribberink, D. Walstra, and W. Kranenburg (2012),
381 Application of a new sediment transport formula within the cross-shore morphodynamic
382 model unibest-tc, in *Proceedings 33rd International Conference on Coastal Engineering*.
- 383 Van Rijn, L. C. (2007a), Unified view of sediment transport by current and waves, i:
384 initiation of motion, bed roughness and bed-load transport, *J. Hydraul. Eng.*, 133,
385 649–667.
- 386 Van Rijn, L. C. (2007b), Unified view of sediment transport by current and waves, ii:
387 suspended transport, *J. Hydraul. Eng.*, 133, 668–689.
- 388 Van Rijn, L. C., D. J. R. Walstra, B. Grasmeijer, J. Sutherland, S. Pan, and J. P. Sierra
389 (2003), The predictability of cross-shore bed evolution of sandy beaches at the time scale
390 of storms and seasons using process-based profile models, *Coastal Eng.*, 47, 297–327.
- 391 Wright, D., J. Boon, S. Kim, and J. List (1991), Modes of cross-shore sediment transport
392 on the shoreface of the Middle Atlantic Bight, *Mar. Geol.*, 96, 19–51.

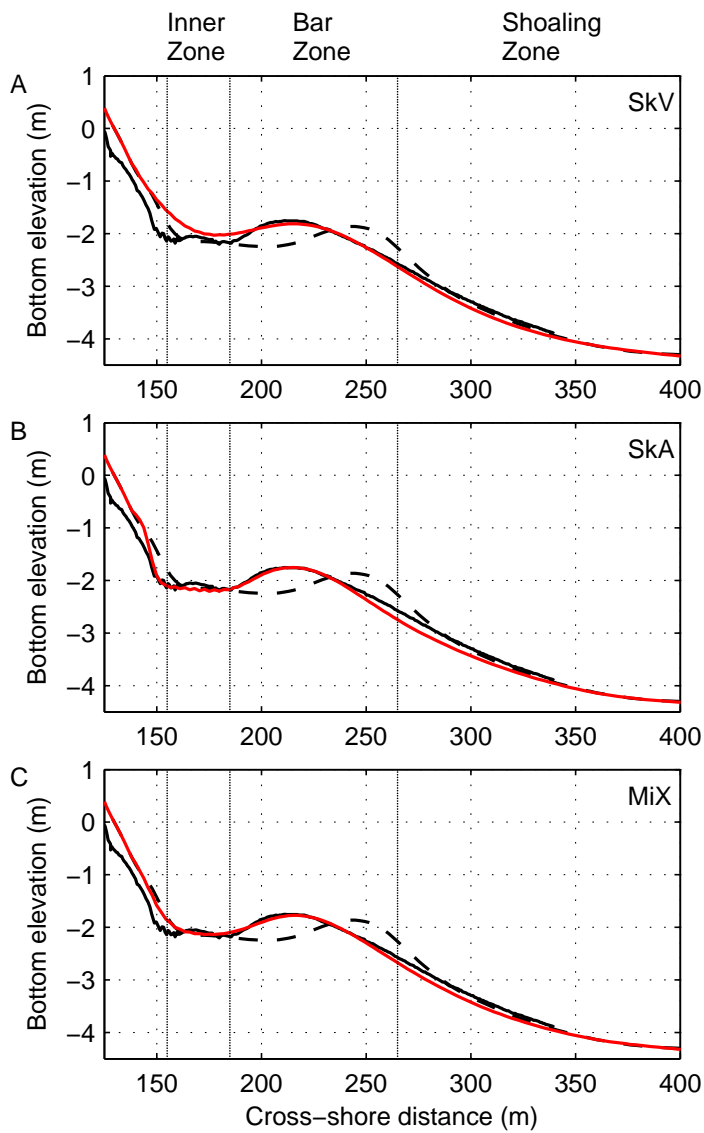


Figure 1. Morphological evolution (red line) of the Duck'94 onshore migration event for A) the SkV transport, B) the SkA transport, and C) the MiX transport. The initial measured profile (21st September, black dashed line), final measured profile (28th September, black solid line) are shown in each panel.

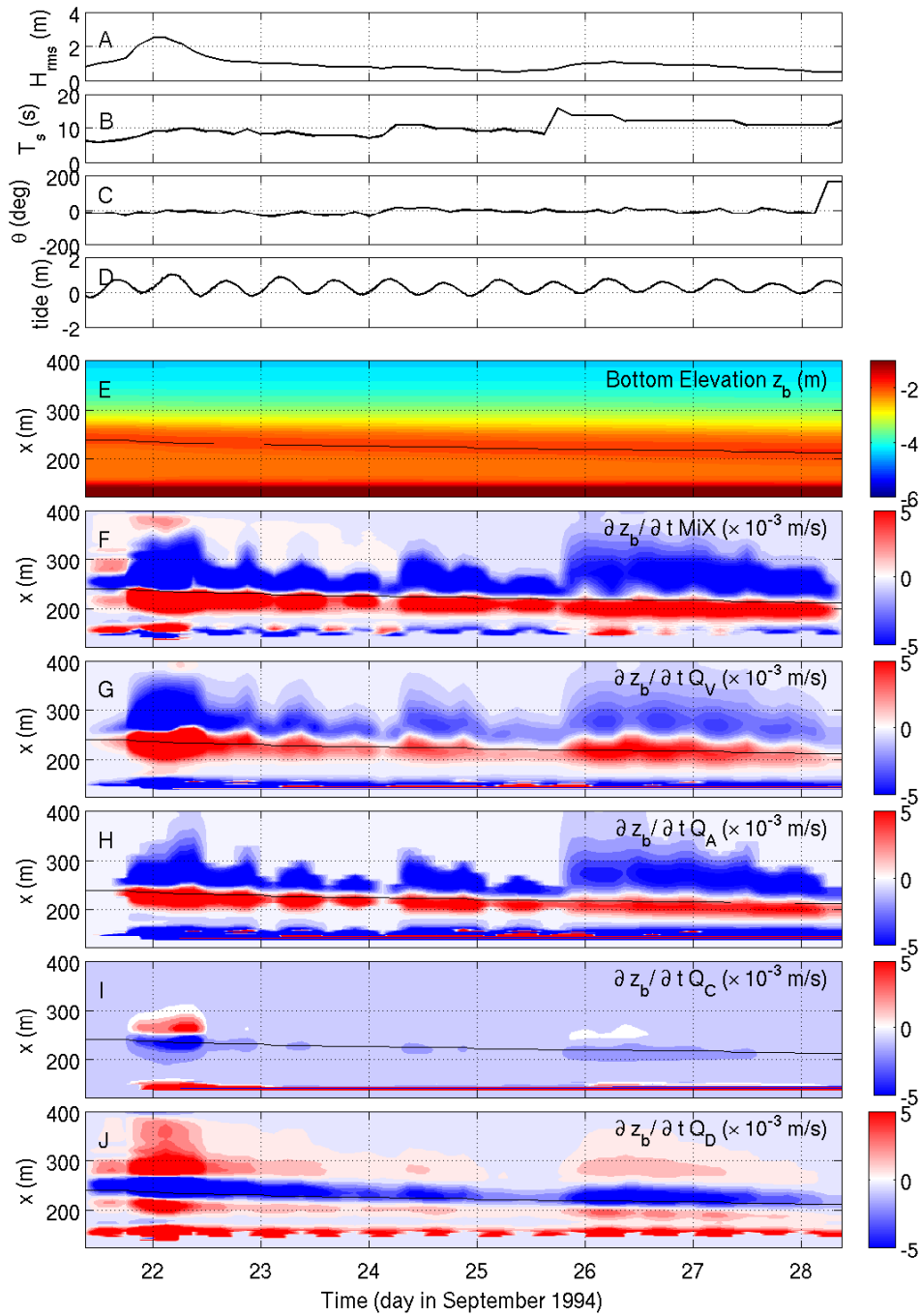


Figure 2. Time series of the observed offshore wave height H_{rms} , period T_p , angle of incidence θ and tide level (panels A to D). Panel E: Bottom evolution z_b during the Duck94 experiment for the MiX transport; panel F: Bottom changes driven by the MiX transport; panels from G to J: Bottom changes driven by each terms of the MiX transport: Q_V , Q_A , Q_C and Q_D respectively. Black solid line indicates the position of the bar crest.

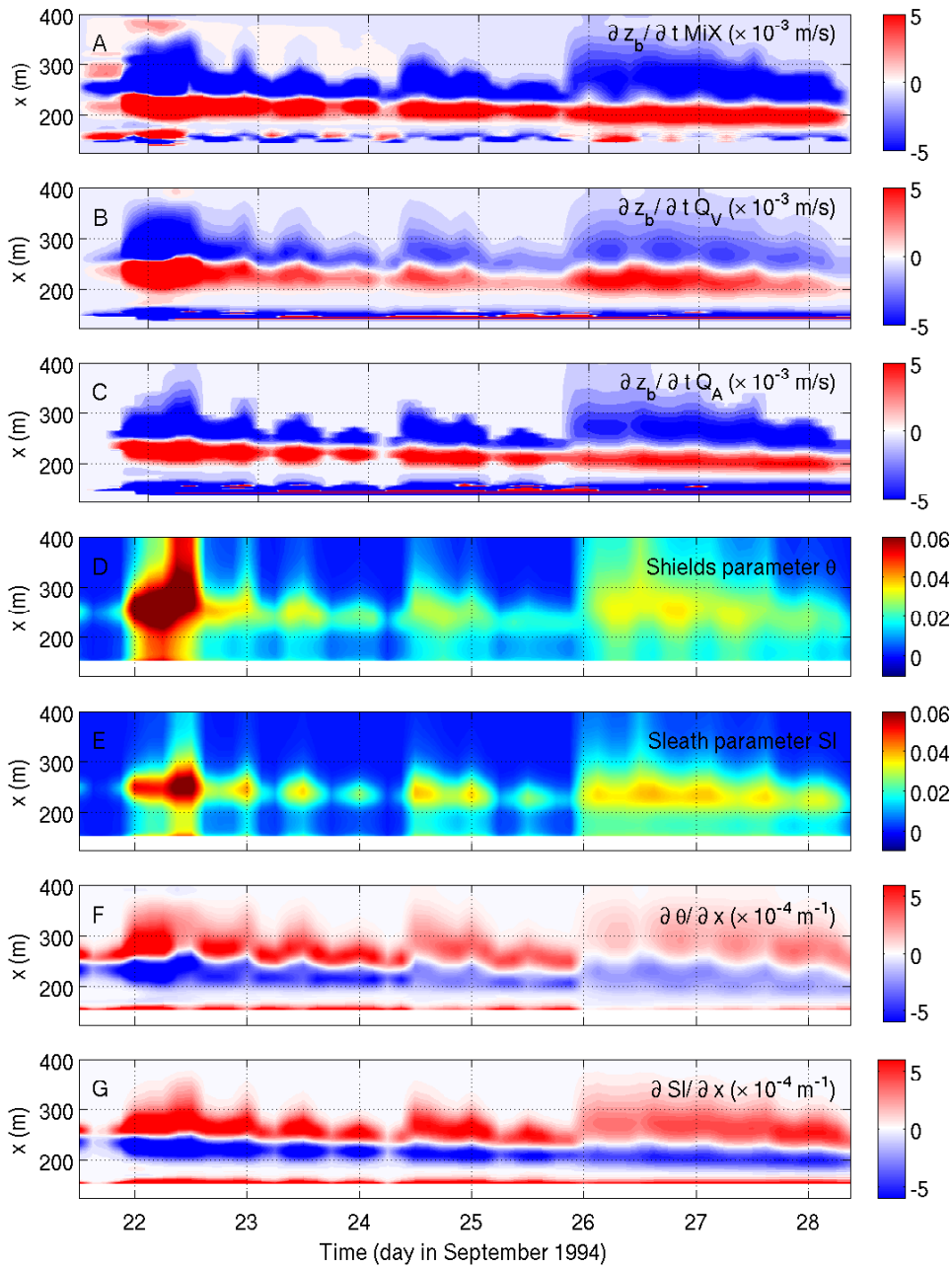


Figure 3. Time series of the bottom changes for the MiX transport, the Q_V term and the Q_A term (panels A to C). Panel D: Shields parameter θ' during the event; panel E: Sleath parameter Sl ; panel F: spatial derivative of θ' , $\partial \theta' / \partial x$; and panel G, spatial derivative of the Sl , $\partial \theta' / \partial x$.

Table 1. Summary of the maximum model skill S and the corresponding $[\alpha_V, \alpha_A, \beta, \gamma]$ parameters at the bar, inner and offshore zones and the total profile, for the SkV, SkA and MiX transport.

	bar	inner zone	offshore zone	full profile	α_V	α_A	β	γ
(x_1, x_2)	S_{bar} (185, 265)	S_{in} (155, 185)	S_{off} (265, 335)	S_{tot} (155, 335)				
<i>SkV</i>	0.965	0.623	0.876	0.604	1.00	0.00	1.00	1.00
<i>SkA</i>	0.955	0.927	0.742	0.744	0.00	1.00	1.00	1.00
<i>MiX</i>	0.981	0.893	0.851	0.816	0.45	0.45	0.40	1.00